ELECTRICAL, THERMAL AND ELECTRO-MAGNETIC ANALYSES OF A 100 kHz INTERLEAVED POWER ELECTRONIC TRANSFORMER

Arya Venugopal – Femi Robert*

Department of Electrical and Electronics Engineering, Faculty of Science and Technology, SRM Institute of Science and Technology, Kattankulathur-603202, Chennai, India

ARTICLE INFO

***Article history*:**
Received: 14.03.2023.
Received in revised form: 29.28.2023.
Accepted: 30.08.2023.

Keywords:
Power electronic transformer
Finite element modelling
Electromagnetic analysis
Electrical analysis
Thermal analysis

DOI: https://doi.org/10.30765/er.2121

Abstract:

In this paper, the finite element electrical, thermal and electro-magnetic analysis of an interleaved power electronic transformer structure operable at 100 kHz is presented. The analysed power electronic transformer structure is modelled with an EE-shaped core and interleaved primary and secondary windings. Electromagnetic analysis was done on the structure to study its properties like magnetic flux density, magnetic field, current density and relative permeability. Electrical and thermal analysis was done on the transformer to study its operating efficiencies and losses in isolation, buck and boost working modes. The analyses were done for different frequencies to ascertain that 100 kHz is the better choice of frequency for the designed power electronic transformer. The results are compared to a non-interleaved power electronic transformer structure to study the improvement obtained in the interleaved model. It was seen that transformer efficiencies of about 99 % could be obtained on using interleaved winding technique rather than non-interleaved method. Finite element modelling software-Altair FLUX was used to simulate the transformer and analytic equations were used to verify the obtained results.

1 Introduction

Transformers are crucial for isolation purposes in high voltage and high-power electrical systems, as they provide proper protection to the circuitry. They also prevent system transients at one side from passing to the other side. Such floating inputs and outputs are much easier to use, because of their compatibility with other circuits as they have separate ground connections [1]. But usage of conventional transformers always poses the problem of increased size and volume of the system. High frequency transformers on the other hand, has a very low volume and weight for their magnetic components. This is because, with increase in frequency, the magnetic energy stored in the transformer core will also increase. That is, at a higher frequency, the same power can be transferred by a smaller transformer [2]. Power Electronic Transformer (PET) is one such emerging transformer, mostly used in isolated switched mode power supplies operating at high frequency [3]. Compared to conventional wire-wound transformers, power electronic transformers have several advantages like reduced height giving a lower profile, larger surface area enabling better heat dissipation, larger magnetic cross-sectional area requiring only fewer turns, smaller winding area, lesser parasitic effects like leakage inductance, lower AC winding resistance and excellent reproducibility [4]–[6]. Power electronic magnetic components have the additional advantage of increasing the stability of the system by enabling it to withstand mechanical vibrations [7], [8]. High efficiency, high power density power electronic transformers are hugely desired in a wide variety of applications that require isolated DC-DC converters, like in electric vehicles, for the vehicles' charging architectures, and drive trains [9], [10]. To obtain these desired features, PET

* Corresponding author
E-mail address: r.femi85@gmail.com

architectures have to be carefully designed. PETs usually have thin copper sheets as windings, either riveted together at the ends, or etched on a PCB in a spiral form [11], [12]. Several other architectures were also designed for the structure of a PET over the years. A magnetic shunt integrated PET structure delivers a wider frequency range of operation for the system [13]. A matrix transformer structure based on variable width winding reduces the current stress, footprint and core losses [14]. A paired layers winding structure minimises the common mode noise in PETs [15]. A fractional turns structure of PET ensures lesser volume and higher power density [16]. Studies have been done even to analyse and model the high frequency fringing losses of PETs [4], [17], [18].

Even though most of these works are focused on mitigating the parasitic losses of the PET like its leakage inductances [19] and stray capacitances [20], [21], many of these are not evaluated for their finite element performance in electromagnetic, electric and thermal aspects. Structural, formational and material modulations in transformers always have an associated effect on their finite element aspects like electromagnetic, electric and thermal performances. So, lack of careful studies and analysis on such aspects will cause performance degradation and stability deterioration not only on the transformers, but also on their associated converters [20]. In this paper, the finite element modelling of a PET structure is designed with an 'interleaved' winding structure. That is, in this structure, the primary and secondary windings of the transformer are arranged in an interleaved design, instead of the conventional 'non-interleaved' or continuous winding arrangement. This will help in eliminating the overlapping between the primary and secondary windings, and thereby in reducing the effect of parasitic components and EMI issues of the PET. Also, such an interleaved arrangement will help in a more proper magnetic flux linkage [22], ensuring lesser leakage inductance in the transformer [23]. The overlapping between windings is avoided by using layers of insulators and PCBs in between, ensuring large spacing between consecutive winding layers.

The studied model was simulated in a finite element modelling (FEM) software, and the results were compared to a conventional non-interleaved power electronic transformer structure to analyse the improvement in the interleaved model. Electromagnetic analysis was done on the structure to study its properties like magnetic flux density, magnetic field, current density and relative permeability. Electrical and thermal analysis was done on the transformer to study its operating efficiencies and losses in isolation, buck and boost working modes. The analyses were done for different frequencies to ascertain that 100 kHz is the best frequency for the designed power electronic transformer. Altair FLUX 2020.1 is the FEM software used in this analysis as it is the most opted software to develop industry standard transformers. This is because, unlike other FEM software, Altair FLUX has automatic geometry building and meshing capabilities combined with advanced solver algorithms, making it easier for users to develop complex winding arrangements employed in primary and secondary sides of transformers. In this work, the multiphysics applications of this software such as steady state and transient AC modelling were used to develop the electromagnetic, electrical and thermal models of the PET structure. The paper is divided into the following sections: section 2 gives the modelling of the PET, section 3 gives the electromagnetic analysis results, section 4 gives the results of electrical analysis of the PET, section 5 gives the thermal analysis results and finally section 6 gives a conclusion of the work.

2 Structure and modelling of interleaved power electronic transformer

The basic structures of the conventional 'non-interleaved' power electronic transformer and studied 'interleaved' power electronic transformer is shown in Figure 1. The PET structure consists of a simple EE core, and two window areas designed to accommodate the windings and printed circuit boards (PCBs). One E part of the core is placed on top of the other with a small air gap of 0.1 mm in between them. Such a small air gap will ensure that the fringing losses created by fringing fluxes in the air gaps are minimised. In conventional non-interleaved PET structure, the windings are arranged in such a way that both the primary and secondary windings are arranged together with insulator layers in between. That is, the windings are in a continuous arrangement with less spacing between similar windings. This can lead to improper magnetic flux linkage in the transformer due to associated leakage inductance. But, in the proposed interleaved winding structure, the primary and secondary windings are placed in an interleaved arrangement and not in a continuous winding structure. Thus, similar windings will not overlap each other, thereby eliminating coupling parasitics of the windings, and other related EMI issues. In the studied design, both the windows are designed similarly with an initial layer of PCB, followed by a stack of primary winding, an insulator strip and secondary winding. Then another PCB layer is placed beneath it, followed by the stack of secondary winding, insulator strip and

primary winding; and finally, another PCB layer at the bottom. So, both the windows have a total of 9 stacked layers each accommodated in them.

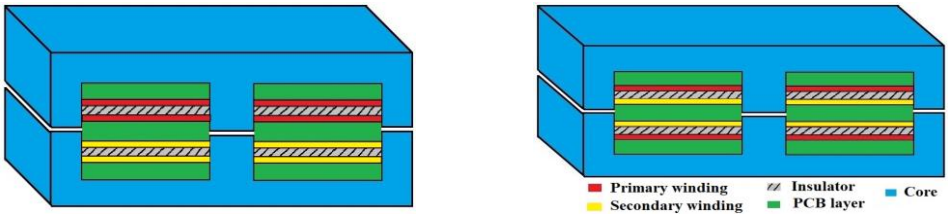

(a) *(b)*

Figure 1. Basic structures of the power electronic transformers (a) Conventional non-interleaved structure (b) Interleaved Structure

Table 1 gives the dimensions of the core and all the different layers of the PET structure. The PET geometry was designed for these required dimensions by developing the various structures in the geometry accordingly using the FEM software's geometry building application. The window slots used in the transformer for arranging various winding layers were designed by using two separate coordinate axes. Several volumes of the PET structure that is to be used for the simulation were developed by implementing Boolean functions like union, addition, assembly and subtraction on the geometry. Further, the boundary limit of the FEM simulation was set by using a parallelopiped infinite box around the PET structure. Through the process of 'meshing', the whole domain of the finite element model is divided into numerous 'nodes' on which various elements of the system are evaluated. The final meshing diagram of the PET simulated is shown in Figure 2. Later, a three-dimensional steady state physical application required for the simulation was defined along with non-meshed coils that superimpose the mesh. Then, various materials were imported for all the different components in the PET geometry. Table 2 describes the specifications of the FEM software used for this study, and Table 3 gives the various materials used for this PET structure.

Table 1. Dimensions of components

Parameter (length × breadth × height)	Dimensions (in mm)
Core	20.32 × 31.75 × 12.34
PCB layer	24.52 × 9.4 × 1.6
Primary winding layer	24.52 × 9.4 × 0.035
Secondary winding layer	24.52 × 9.4 × 0.035
Insulator layer	24.52 × 9.4 × 0.5

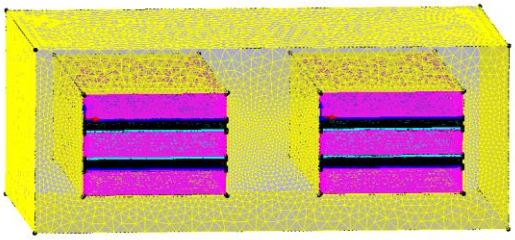

Figure 2. Meshing of the PET structure

Table 2. Specifications of the FEM software used for the study

Parameter	Description
Software used for FEM	Altair FLUX (Version 2020.1)
Software used for importing materials	Material Manager (Version 1.2)
Defined physical application	Stead State AC application in 3D
Mesh order implemented	First order meshing
Number of domain nodes	3,13,522
Excellent quality nodes (%)	63.45
Good quality nodes (%)	26.09
Poor quality nodes (%)	10.46

Table 3. Materials used for different regions of the PET structure

Region	Material	Material name from FLUX Material Manager
Core	Ferrite	MAGNETICSINCUSA_FERRITE_J_5000_MU_DC
Coils	Copper	FLU_COPPER
PCB	Polyamide	FLU_POLYAMIDE
Insulators	Porcelain	FLU_PORCELAIN

The mathematical description of the FEM method is based on the electromagnetic evaluations performed using the fundamental magnetic field and voltage gradient computations at all the nodes of the finite element model, and is given as follows:

$$\nabla \frac{1}{\mu_0} . \nabla \vec{H} + \sigma \left(\vec{E}, \vec{B} \right) \frac{\partial \vec{H}}{\partial t} = -\sigma \left(\vec{E}, \vec{B} \right) \nabla V \tag{1}$$

where $\vec{H}$, $\vec{E}$ and $\vec{B}$ are the magnetic field, electric field and magnetic flux vectors respectively, and ∇V is the voltage gradient.

3 Electromagnetic analysis of the power electronic transformer

Electromagnetic analysis of the novel power electronic transformer structure was performed with the specifications of a standard industrial power electronic transformer [24] to verify that the improved interleaved winding structure did not affect electromagnetic aspects of the transformer.

A ferrite core was used as the magnetic core of the transformer. The function of a magnetic core in a power electronic transformer is to lead the magnetic flux. For a sinusoidal wave input, the peak magnetic flux density B_{max} of a power electronic transformer can be assessed with the formula [24], [25]:

$$B_{max} = \frac{V}{4.44 \times f \times N \times A_e} \tag{2}$$

where V is the rms value of the input voltage (in V), f is the frequency of operation (in Hz), N is the number of primary windings, and A_e is the effective area of the core (in m^2). With a frequency of 100 kHz, area of 250 mm^2 [24], voltage of 100 V, and 2 primary windings, the calculated value of B_{max} was found to be 0.45 T. The B_{max} of a non-interleaved power electronic transformer structure simulated was found to around 0.429 T as seen in Figure 3, which is less than the calculated maximum flux density value. Thus, the transformer core is optimised with major parts of the core working at a magnetic flux density closer to the B_{max} value. The direction of magnetic flux density distribution of the transformer shown in Figure 4. The magnetic field distribution of

the model shown in Figure 5 is also likewise, where the effects vary from near the window slots holding the current carrying windings, to the rest of the core.

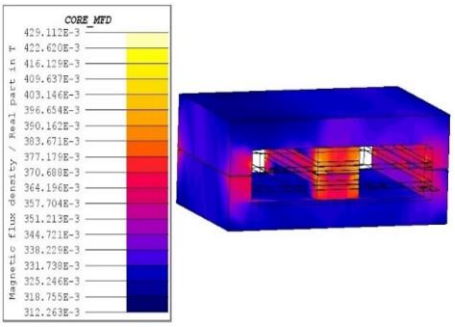

Figure 3. Magnetic flux density distribution

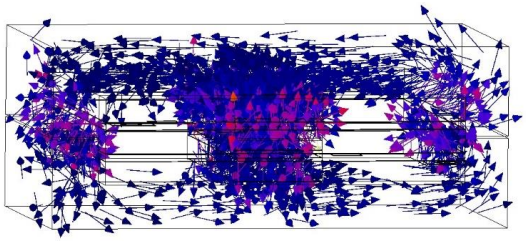

Figure 4. Direction of magnetic flux density distribution

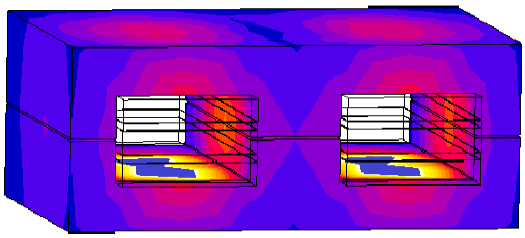

Figure 5. Magnetic field distribution

The variation of relative permeability of the core material is shown in Figure 6. The relative permeability of ferrite material used in a conventional power electronic transformer [24] is 21972.757, and from the distribution, it is seen that the core design is optimised as major parts of the core is working around this permeability value. Table 4 summarises the comparison results of the electromagnetic properties of both non-interleaved and interleaved transformer design.

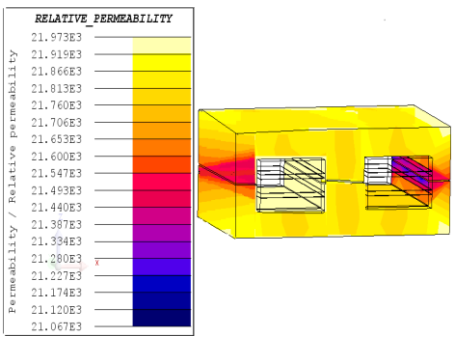

Figure 6. Relative permeability distribution

Table 4. Comparison of electro-magnetic properties of PETs

Parameter	B_{max} (T)	Relative Permeability
Analytic Values	0.45	21927.7
Non-interleaved PET	0.345	18365
Interleaved PET	0.429	21919
Percentage variation of non-interleaved PET (%)	23.33	16.25
Percentage variation of interleaved PET (%)	4.66	0.03

It is observed that for non-interleaved PET, a variation of about 23 % is found in simulated B_{max} values when compared to the calculated B_{max} values. Whereas, for the interleaved PET structure, B_{max} values vary only by about 4 %. On comparing the relative permeabilities of the core, it is seen that non-interleaved PET shows a 16% variation from the calculated relative permeability, whereas interleaved structure shows only a slight 0.03 % variation. Thus, it can be concluded that the design of the interleaved PET with superior winding advantages improved the electromagnetic aspects of the PET.

4 Electrical analysis of the power electronic transformer

The simplified electrical model of the power electronic transformer implemented in the simulation is shown in Figure 7 [24].

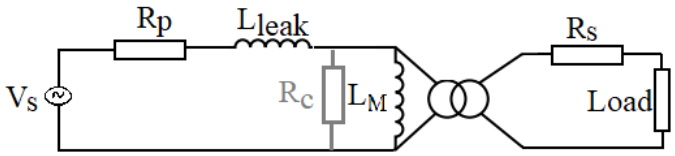

Figure 7 Simplified electrical model of the transformer

R_p and R_s denotes the primary and secondary resistances respectively, R_c shows the resistance corresponding to core losses, L_{leak} denotes the combined leakage inductances of both the primary and secondary side, and L_M denotes the magnetizing inductance of the transformer. A sinusoidal voltage of rms value 100 V and 100 kHz frequency is supplied to the primary side, and a load of 2 kW and 50 Ω is connected at the secondary side. The electrical specifications of the power electronic transformer modelled are given in Table 5 [26].

Table 5. Electrical parameters of the PET

Specification	Value
Input Voltage, V_s	100 V
Load rating	2 kW, 50 Ω
Winding Ratio (N_p : N_s)	2 : 3
Frequency	100 kHz
L_{leak}	150 nH
L_M	128 µH

The power electronic transformer can have three types of operation; buck, isolation or boost. The proposed winding structure is designed for a turns ratio of 2 : 3 in isolation operation. That is, when the ratio of number of primary turns (N_p) to the number of secondary turns (N_s) is 2 : 3, the output voltage obtained will be equal to the input voltage. In buck operation, the voltage applied at the input will be stepped down at the output side. To obtain this, the designed N_s (3) should be maintained less than or equal to the designed N_p (2). In boost

operation, the voltage applied at the input will be stepped up at the output side, and for this operation the designed N_s should be greater than the designed N_p.
The core power losses can be assessed with the formula [24]:

$$P_{core}=2.425 \times 10^{-6} \times (B_{max})^{2.5891} \times (f)^{1.6677} \quad (3)$$

where P_{core} is the ferrite core power losses (in W).

Winding resistance is an important parameter in evaluating the copper losses due to the current flow through the windings. Winding resistance can be calculated with the formula [24]:

$$R_{DC}= \rho_{20^oC} \times \frac{l}{A} \quad (4)$$

where R_{DC} is the winding resistance at 20 °C (in Ω), ρ_{20^oC} is the electrical resistivity of copper at room temperature in (in Ωm), l is the length of the winding (in m), and A is the cross section of the conductor used for the winding (in m^2).
The electrical resistance is dependent on the working temperature of the winding. For windings made of copper, the resistance at temperature T can be approximated with the formula [24]:

$$R = R_{DC} \times [1 + (3.90 \times 10^{-3}) \times (T - 20)] \quad (5)$$

where R is the winding resistance at working temperature (in Ω) and T is the working temperature (in °C). Thus, the total I^2R losses of the transformer can be estimated with this resistance.
Medium power PETs are usually designed for frequencies ranging from a few kilohertz to a few hundred kilohertz. Table 6 gives the output observations from the simulations in buck, isolation and boost operations of the transformer in three different frequencies (1 kHz, 50 kHz and 100 kHz) to find the better choice of frequency for the designed transformer. Isolation mode operation was obtained for $N_p : N_s = 2 : 3$, buck operation was obtained for $N_p : N_s = 2 : 2$ (that is, $N_s < 3$) and boost operation was obtained for $N_p : N_s = 2 : 4$ (that is, $N_s > 3$).

Table 6. Electrical Parameters of the PET

Parameter	f = 1 kHz			f = 50 kHz			f = 100 kHz		
Operation mode	Buck	Isolation	Boost	Buck	Isolation	Boost	Buck	Isolation	Boost
Turns Ratio	2:2	2:3	2:4	2:2	2:3	2:4	2:2	2:3	2:4
Output Voltage (V)	72.83	108.39	145.67	72.44	108.83	144.89	71.90	108.14	143.81
Output Current (A)	28.89	21.87	13.86	28.74	21.76	13.78	28.52	21.62	14.14
P_{core} (W)	524.28	524.28	524.28	131.25	131.25	131.25	7.52	7.52	7.52
P_{copper} (W)	9.01	5.16	2.07	8.92	5.11	2.05	8.78	5.04	2.16
Total losses (W)	533.29	529.45	526.35	140.17	136.36	133.30	16.31	12.57	9.68
Efficiency (%)	73.33	73.52	73.68	92.99	93.18	93.33	99.18	99.37	99.51

It is seen that the losses and efficiencies are obtained in a desirable range for the PET design in 100 kHz operation. The results show a very high efficiency (more than 99 %) for the designed transformer model in all the three types of operation, which is in accordance with the desired efficiency for a conventional medium power PET [24]. Another observation from the results is that copper losses of the power electronic transformer is always very small when compared to the core losses. This is because, unlike conventional wire-wound

transformers, power electronic transformers have a very high ratio of ferrite to copper volumes. That is, they will typically comprise of a core with a larger cross section area, along with windings having smaller number of turns [27]. Thus, copper losses of a power electronic transformer will always be very small. Also, the electrical analysis results of a non-interleaved transformer with the same specifications were compared with the proposed interleaved transformer, to compare the improvement in losses and efficiencies in all three modes of operation. The results are shown in Figure 8. It was seen that the losses and efficiencies of the proposed transformer was better than the non-interleaved transformer in all three operating modes.

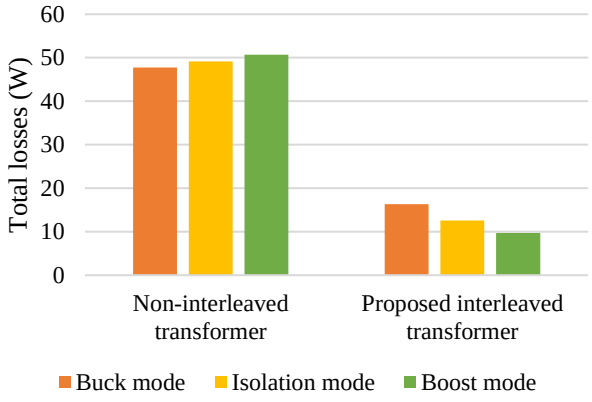

(a)

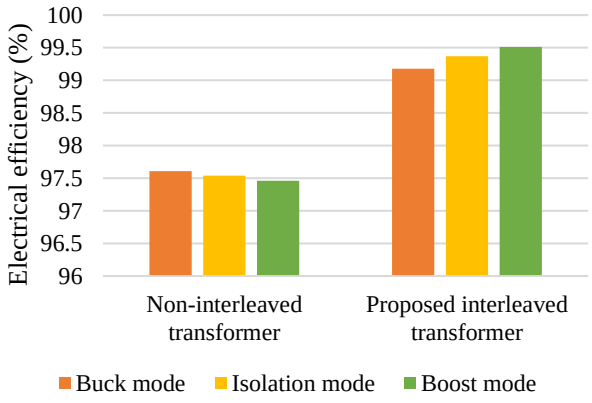

(b)

Figure 8. Comparison of electrical analysis results of non-interleaved and proposed interleaved transformers (a) Comparison of losses (b) Comparison of efficiencies

5 Thermal analysis of the power electronic transformer

Thermal analysis is very important for studying the reliable performance of the transformer in all working conditions. For studying this new PET design, the 3D steady state AC magnetic application of the FEM software Altair FLUX was coupled with transient thermal application. A transient application was included to study the effects of transient heating. Transient heating occurs as a result of 'Joule effect' of induced currents. Joule effect is basically the I^2R heating caused due to current flow through a resistor, and the induced currents results from the eddy current generation due to heating. The temperature gradient of the transformer core is shown in Figure 9. An average temperature rise of around 11 K per metre is seen in the transformer core. The operable range of a typical power electronic transformer with heat sink dissipation is between 218 to 400 K [24]. Thus, the obtained temperature rise is tolerable. The direction of this temperature gradient is shown in Figure 10. The temperature variation starts from near the windings which act as the thermal source, and extends outwards away from the source. The thermal flux on the core surfaces is shown in Figure 11. It is seen that, as

expected, the flux is higher in the centre of the core near the windings, and lower towards the farther ends of the surface.

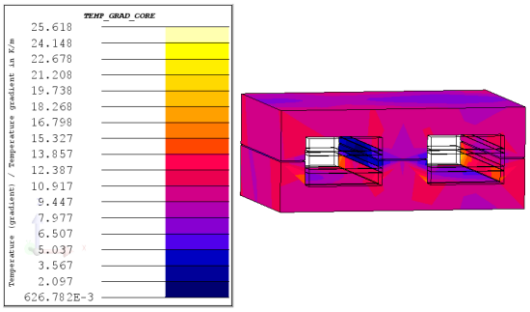

Figure 9. Temperature gradient distribution

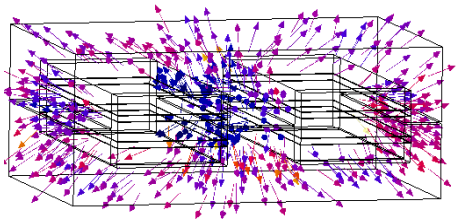

Figure 10. Direction of temperature gradient distribution

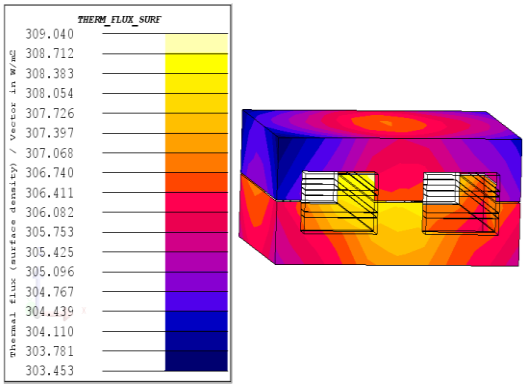

Figure 11. Thermal flux of core surface

Thermal efficiency of a transformer has to be analysed well and improved to help reduce the energy usage and thereby costs. In FEM studies, thermal efficiency can be calculated by calculating the mean power and mean losses, by using separate sensors for these in addition to several temperature sensors on the structure. The power sensor will calculate the thermal flux density and the losses sensor gives an integration of the surface heat density to find the losses by convection, radiation, eddy currents etc.
With these sensor outputs, thermal efficiency can be calculated as [28]:

$$\eta_{thermal} = \frac{P_{mean} - L_{mean}}{P_{mean}} \times 100 \tag{6}$$

where $\eta_{thermal}$ is the thermal efficiency (in %), P_{mean} is the mean value of dissipated power in the volume during all heat intervals, and L_{mean} is the mean value of thermal losses on the surfaces during all heat intervals. P_{mean} is computed as the losses by Joule's effect; that is, it gives the thermal flux density of the volume. L_{mean} is calculated as the integration of surface heat density of the faces; that is, it gives the losses by convection, radiation, eddy currents etc.

Table 7 gives the P_{mean}, L_{mean} and thermal efficiencies calculated for the model with three different frequencies in which medium power PETs are conventionally designed. It is seen that the thermal efficiency is the highest in the design with 100 kHz, along with lowest power dissipation and thermal losses. This is in accordance with the desired thermal efficiency (more than 99%) of a conventional medium power PET [24]. Also, the thermal results of a non-interleaved transformer simulated with similar specifications is compared with the thermal results of the proposed interleaved transformer in all three operating modes, and the results are shown in Figure 12. It was seen that the thermal efficiency of the proposed interleaved transformer is higher than the non-interleaved transformer in all modes.

Table 7. Calculated thermal parameters of the PET

Parameter	f = 1 kHz			f = 50 kHz			f = 100 kHz		
Operation mode	Buck	Isolation	Boost	Buck	Isolation	Boost	Buck	Isolation	Boost
Turns Ratio	2:2	2:3	2:4	2:2	2:3	2:4	2:2	2:3	2:4
P_{mean}	1998.76	1295.81	841.44	1001.16	648.91	421.82	502.88	325.45	211.41
L_{mean}	495.75	325.61	211.36	100.11	50.81	41.23	1.37	1.16	1.02
$\eta_{thermal}$	75.19	74.87	74.88	90.01	92.16	90.22	99.72	99.64	99.51

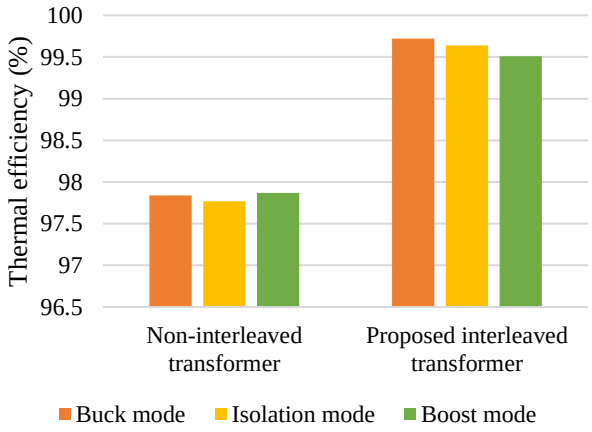

Figure 12. Comparison of thermal efficiencies of non-interleaved transformer and proposed interleaved transformer

6 Conclusion

The finite element analysis of a non-interleaved and interleaved power electronic transformer is presented in this paper using Altair Flux software. The power electronic transformer structure is designed with an EE core, which is designed to accommodate stacked layers of printed circuit boards and insulations, with non-interleaved or interleaved primary and secondary windings. Electromagnetic, electrical and thermal analysis were done on the model. Electromagnetic analysis on both the transformer types revealed that the interleaved structure resulted in a more precise magnetic flux density and permeability values (with variations as less as 4.66 % and 0.03 % respectively) when compared to the non-interleaved PET (with variations of about 23.33 % and 16.25 % respectively). Electrical and thermal efficiencies of the interleaved PET structure was obtained

to be more than 99% in isolation, buck and boost operations, whereas the non-interleaved PET structure gives only about 97 % electrical and thermal efficiencies. Thus, when compared to the conventional non-interleaved design, the interleaved PET design gave better finite element analyses results along with the added advantages of the superior winding method. All the analyses yielded the best results for transformer operation at 100 kHz, thus making it the better frequency choice for this medium power PET design.

Acknowledgment

This work is part of SRMIST Selective Excellence Research Initiative-2021: "DCFCEVB".

References

[1] A. Parisi, E. Ragonese, N. Spina, and G. Palmisano, "Galvanically Isolated DC-DC Converter Using a Single Isolation Transformer for Multi-Channel Communication," *IEEE Trans. Circuits Syst. I Regul. Pap.*, vol. 67, no. 12, pp. 4434–4444, 2020, doi: 10.1109/TCSI.2020.3007314.

[2] "Design Considerations for High Frequency Transformers," *Agile Magnetics*, 2021. https://www.agilemagco.com/blog/your-source-high-frequency-transformers/.

[3] G. K. Y. Ho *et al.*, "High-Frequency PCB Winding Transformer With Integrated Inductors for a Bi-Directional Resonant Converter," *IEEE Trans. Power Electron.*, vol. 34, no. 9, pp. 653–663, Apr. 2022, doi: 10.1109/TTE.2021.3121172.

[4] Z. Ouyang and M. A. E. Andersen, "Overview of Planar Magnetic Technology—Fundamental Properties," *IEEE Trans. Power Electron.*, vol. 29, no. 9, pp. 4888–4900, 2014, doi: 10.1109/TPEL.2013.2283263.

[5] S. M. Djuric and G. M. Stojanovic, "A Compact Planar Transformer With an Improved Winding Configuration," *IEEE Trans. Magn.*, vol. 50, no. 11, pp. 1–4, 2014, doi: 10.1109/TMAG.2014.2321630.

[6] H. Y. Lu, J. G. Zhu, and S. Y. R. Hui, "Experimental determination of stray capacitances in high frequency transformers," *IEEE Trans. Power Electron.*, vol. 18, no. 5, pp. 1105–1112, 2003, doi: 10.1109/TPEL.2003.816186.

[7] L. Dixon, "Designing Planar Magnetics," *Texas Instruments*, 2020. https://www.ti.com/download/trng/docs/seminar/Topic4LD.pdf.

[8] L. Dalessandro, F. da S. Cavalcante, and J. W. Kolar, "Self-Capacitance of High-Voltage Transformers," *IEEE Trans. Power Electron.*, vol. 22, no. 5, pp. 2081–2092, 2007, doi: 10.1109/TPEL.2007.904252.

[9] Z. Zhang, C. Liu, M. Wang, Y. Si, Y. Liu, and Q. Lei, "High-Efficiency High-Power-Density CLLC Resonant Converter with Low-Stray-Capacitance and Well-Heat-Dissipated Planar Transformer for EV On-Board Charger," *IEEE Trans. Power Electron.*, vol. 35, no. 10, pp. 10831–10851, 2020, doi: 10.1109/TPEL.2020.2980313.

[10] N. G. Ali Mamizadeh, Bestoon Ahmed Mustafa, "Planar Flyback Transformer Design for PV Powered LED Illumination," *Int. J. Renew. Energy Res.*, vol. 11, no. 1, 2021.

[11] J. Zhang, J. Liu, J. Yang, N. Zhao, Y. Wang, and T. Q. Zheng, "A Modified DC Power Electronic Transformer Based on Series Connection of Full-Bridge Converters," *IEEE Trans. Power Electron.*, vol. 34, no. 3, pp. 2119–2133, 2019, doi: 10.1109/TPEL.2018.2842728.

[12] V. K. N, "Comparison of Planar Transformer Architectures and Estimation of Parasitics for High Voltage Low Power DC-DC Converter," *2018 IEEE Int. Conf. Power Electron. Drives Energy Syst.*, pp. 1–6, 2018.

[13] M. Li, Z. Ouyang, and M. A. E. Andersen, "High-Frequency LLC Resonant Converter with Magnetic Shunt Integrated Planar Transformer," *IEEE Trans. Power Electron.*, vol. 34, no. 3, pp. 2405–2415, 2019, doi: 10.1109/TPEL.2018.2842029.

[14] M. Dai, X. Zhang, H. Li, Di. Zhou, Y. Wang, and Di. Xu, "LLC Converter with an Integrated Planar Matrix Transformer Based on Variable Width Winding," *2019 22nd Int. Conf. Electr. Mach. Syst. ICEMS 2019*, 2019, doi: 10.1109/ICEMS.2019.8922483.

[15] M. A. Saket, M. Ordonez, M. Craciun, and C. Botting, "Improving Planar Transformers for LLC Resonant Converters: Paired Layers Interleaving," *IEEE Trans. Power Electron.*, vol. 34, no. 12, pp. 11813–11832, 2019, doi: 10.1109/TPEL.2019.2903168.

[16] Y. C. Liu *et al.*, "Design and Implementation of a Planar Transformer with Fractional Turns for High Power Density LLC Resonant Converters," *IEEE Trans. Power Electron.*, vol. 36, no. 5, pp. 5191–5203, 2021, doi: 10.1109/TPEL.2020.3029001.

[17] R. Shafaei, M. C. G. Perez, and M. Ordonez, "Planar Transformers in LLC Resonant Converters: High-Frequency Fringing Losses Modeling," *IEEE Trans. Power Electron.*, vol. 35, no. 9, pp. 9634–9651, 2020, doi: 10.1109/TPEL.2020.2971424.

[18] J. J. Shea, "Transformer and Inductor Design Handbook, 3rd Ed. [Book Review]," *Electr. Insul. Mag. IEEE*, vol. 21, p. 61, Feb. 2005, doi: 10.1109/MEI.2005.1389284.

[19] A. Venugopal and F. Robert, "Analysis of a Non-overlapping Interleaved Planar Transformer Winding Structure with Reduced Parasitic Effects," *Iran. J. Sci. Technol. Trans. Electr. Eng.*, vol. 3, 2022, doi: 10.1007/s40998-022-00507-3.

[20] M. Pahlevaninezhad, P. Das, J. Drobnik, P. Jain, A. Bakhshai, and G. Moschopoulos, "A novel winding layout strategy for planar transformer applicable to high frequency high power DC-DC converters," *IEEE Energy Convers. Congr. Expo. Energy Convers. Innov. a Clean Energy Futur. ECCE 2011, Proc.*, pp. 3786–3791, 2011, doi: 10.1109/ECCE.2011.6064283.

[21] Z. Ouyang, O. C. Thomsen, and M. A. E. Andersen, "Optimal design and tradeoff analysis of planar transformer in high-power dc-dc converters," *IEEE Trans. Ind. Electron.*, vol. 59, no. 7, pp. 2800–2810, 2012, doi: 10.1109/TIE.2010.2046005.

[22] M. Li, Z. Ouyang, and M. A. E. Andersen, "Discovery of the Nearly Zero Flux between Two Parallel Conductors in Planar Transformers," *IEEE Trans. Power Electron.*, p. 1, 2021, doi: 10.1109/TPEL.2021.3093171.

[23] R. Yu, T. Chen, P. Liu, and A. Q. Huang, "A three–dimensional (3D) winding structure for planar transformers and its applications to LLC resonant converters," *IEEE J. Emerg. Sel. Top. Power Electron.*, p. 1, 2021, doi: 10.1109/JESTPE.2021.3052712.

[24] S. Marchio, "Designing With the PLA51 Planar Transformer for Enhanced Power Density and Efficiency," in *Vishay Electronics-Transformer Application Note*, Vishay Sfernice Ltd., 2017.

[25] S. J. Chapman, *Electric machinery fundamentals*. Fifth edition. New York : McGraw-Hill, [2012] ©2012, 2012.

[26] Vishay Electronics, "PLA51LA32 Medium Power Planar Transformer 1 kW to 3 kW," *Vishay Sfernice Ltd.*, 2020. http://www.farnell.com/datasheets/2245234.pdf.

[27] S. Ben-Yaakov, "The Benefits of Planar Magnetics in OF Power Conversion Planar Magnetics (PM) : The Technology that Meets the Challenges of HF Switch and Resonant Mode Power Conversion," *Mater. Sci.*, 2006.

[28] "Magneto Thermal Application - 3D technical exmaple," in *Altair Flux*, 2020.